Original article

Improving the accuracy of analytical relationships for mechanical properties of additively manufactured lattice structures

R. Hedayati[1*], N. Ghavidelnia[2], M. Sadighi[2], M. Bodaghi[3]

[1]Novel Aerospace Materials Group, Faculty of Aerospace Engineering, Delft University of Technology (TU Delft), Kluyverweg 1, 2629 HS Delft, the Netherlands

[2]Department of Mechanical Engineering, Amirkabir University of Technology (Tehran Polytechnic), Hafez Ave, Tehran, Iran

[3]Department of Engineering, School of Science and Technology, Nottingham Trent University, Nottingham NG11 8NS, United Kingdom

[1] Corresponding author, email addresses: r.hedayati@tudelft.nl, rezahedayati@gmail.com, Tel: +31 (0)15 27 88777

ABSTRACT

Porous implants must satisfy several physical and biological requirements in order to be promising materials for orthopedic application: they should have the proper levels of stiffness, permeability, and fatigue resistance and in proximity to how much they are in bone tissues. In recent years, several experimental, numerical, and analytical studies have been carried out on the influence of unit cell geometry on such properties. Even though experimental and numerical techniques can effectively study and predict the behavior of different micro-structure, they lack the ease the analytical relationships provide for such predictions. Even though it is well-known that Timoshenko beam theory gives much better accuracy in predicting the deformation of a beam (and as a result lattice structures), many of the already-existing relationships in the literature have been derived based on Euler-Bernoulli beam theory. The question that arises here is that can there be a convenient way to convert the already-existing relationships based on Euler-Bernoulli to relationships based on Timoshenko beam theory without the need to rewrite all the derivations from the starting point. In this paper, this question is addressed and answered, and a simple approach is presented. This technique is applied to six unit cells for which Euler-Bernoulli analytical relationships could be found in the literature, but Timoshenko theories could not be found: BCC, hexagonal packing, rhombicuboctahedron, diamond, truncated cube, and truncated octahedron. The results of this study demonstrated that converting analytical relationships based on Euler-Bernoulli to equivalent Timoshenko ones can decrease the difference between the analytical and numerical values for one order of magnitude which is a significant improvement in accuracy of the analytical formulas. The methodology presented in this study is not only beneficial to the already-existing analytical relationships but also facilitates derivation of accurate analytical relationships for other, yet unexplored, unit cell types.

Keywords: Mechanical properties; Euler-Bernoulli beam theory; Timoshenko beam theory; analytical relationship; Finite element method

1. Introduction

Recently, partially or fully porous load-bearing implants have been proposed to replace the traditionally solid implants in case of large bone defects. While metallic foams manufactured by traditional techniques such as powder metallurgy [1], investment casting [2], and space-holder [3] have found their way in this field, they all lack a good controllability over the microstructural geometry of the implant which affects its static mechanical properties [4], fatigue resistance [5, 6], and biological response [7]. Recent blast in the application of additive manufacturing (AM) in this field has opened the possibility of manufacturing porous implants with arbitrary micro-architecture. AM makes it possible to manufacture open-cell (i.e. permeable) porous materials with precisely designed microstructure both in micro- and macro- scales [8].

The porous implants should satisfy many physical and biological requirement in order to be in optimal state for biomedical application: they should have the right levels of stiffness, permeability, and fatigue resistance and in proximity to how much they are in bone tissues. This is especially crucial to avoid undesired consequences of very stiff solid metals which can cause problems such as stress shielding [9].

The regular porous biomaterials are usually made of repeating elements known as unit cells. The mechanical, physical, and biological properties of the implant are determined by three main characteristics of the unit cell they are made of: the shape of the cells, their size, and their relative density (which is defined as the ratio of space occupied by the solid material).

In recent years, several experimental [10-14], numerical [15-20], and analytical [21-25] studies have been dedicated to studying the influence of unit cell shape on such properties. Even though experimental and numerical techniques can effectively study and predict the behavior of different micro-structure, they lack the ease the analytical relationships provide for such predictions. Analytical relationships have several benefits: they can be used for validation of numerical or experimental results, they can be implemented in Machine Learning or Artificial Intelligence algorithms to construct optimally-designed patient-specific implants, and they can give a clear and quick indication of what properties have the most contribution in each of the mechanical properties of a regularly repeated lattice structure.

Previously, analytical relationships for elastic properties (elastic modulus, Poisson's ratio, and yield stress) of different unit cells such as body-centred cubic (BCC) [26], cube [27, 28], diamond [21], hexagonal packing [29], iso-cube [30], octahedral [22], rhombic dodecahedron [23, 25], rhombicuboctahedron [24], truncated cube [27], truncated cuboctahedron [31], and truncated octahedron [32] have been derived. In the literature, relationships for octahedral [22], rhombic dodecahedron [25], and truncated cuboctahedron [31] have been derived based on both Euler-Bernoulli and Timoshenko beam theories. However, for the rest of the above-mentioned geometries the relationships are only derived based on Euler-Bernoulli beam theory. The question that arises here is whether or not there can be a convenient way to convert the already-existing relationships based on Euler-Bernoulli to relationships based on Timoshenko beam theory without the need to rewrite all the derivations from the starting point.

In this study, we try to answer that question by presenting a technique to convert the already-existing Euler-Bernoulli analytical relationships to equivalent Timoshenko ones. This technique is used to convert Euler-Bernoulli elastic relationships including elastic modulus, Poisson's ratio, and yield stress of any porous material (E, σ_y, ν). The efficiency of this technique is evaluated in six unit cells: BCC, hexagonal packing, rhombicuboctahedron, diamond, truncated cube, and truncated octahedron. Numerical simulations are also carried out using finite element (FE) modelling to evaluate if the new technique gives better accuracy in the analytical results. Moreover, experimental data points from previous studies are used for validation of the proposed technique.

2. Materials and methods

2.1. Euler-Bernoulli beam theory

For a beam under no distributed load, the Euler–Bernoulli beam equation can be written as

$$\frac{d^4 w}{dx^4} = 0 \tag{1}$$

where w is the deflection. The solution to this differential equation can be expressed as:

$$w = c_0 + c_1 x + c_2 x^2 + c_3 x^3 \tag{2}$$

where constants $c_0 - c_3$ must be determined by applying certain boundary conditions. For a cantilever Euler-Bernoulli beam with a point load P at its end, we have

$$\delta = \frac{Fl^3}{3E_s I} \qquad and \qquad \theta = \frac{Fl^2}{2E_s I} \tag{3}$$

and for a cantilever beam with a concentrated moment M at its end, the displacement and rotation are obtained as

$$\delta = \frac{Ml^2}{2E_s I} \qquad and \qquad \theta = \frac{Fl}{E_s I} \tag{4}$$

In beams that the angle of the free end does not change during the deformation (e.g. the beams of the lattice structure considered in this study), the rotations produced by the lateral load F and moment M must be equal and opposite from which the value of M can be identified:

$$\frac{Fl^2}{2E_s I} = \frac{Ml}{E_s I} \qquad \rightarrow \qquad M = \frac{Fl}{2} \tag{5}$$

While force F tends to increase the lateral displacement, moment M tends to reduce the deflection. The total deflection caused by force F and moment M is then

$$\delta = \frac{Fl^3}{3E_s I} - \left(\frac{Fl}{2}\right)\frac{l^2}{2EI} = \frac{Fl^3}{12EI} \tag{6}$$

Rewriting (6) as a function of F gives (see Figure 2a)

$$F = \frac{12E_sI}{l^3}\,\delta \tag{7}$$

According to Eq. (5), we will have $M = \frac{6E_sI}{l^2}\,\delta$. Similarly, the axial force required to displace the end of a rod for u is AE_su/l (see Figure 2c). The equations for a cantilever beam with rotation but with no displacement in the end can be obtained in a similar manner and the results are shown in Figure 2b.

2.2. Timoshenko beam theory

Now, we try to find how the moments and forces shown in Figure 2a-b are changed due to change in the beam theory. The Timoshenko beam theory takes into account shear deformation and rotational inertia effects, making it suitable for describing the behaviour of short beams. For a homogenous beam of constant cross-section, the Timoshenko beam governing equations are:

$$\frac{d^2}{dx^2}\left(E_sI\frac{d\varphi}{dx}\right) = q(x,t) \tag{8}$$

$$\frac{dw}{dx} = \varphi - \frac{1}{\kappa AG_s}\frac{d}{dx}\left(E_sI\frac{d\varphi}{dx}\right)$$

where φ is the angle of rotation of the normal to the mid-surface of the beam, w is the displacement of the mid-surface in the z-direction, and κ is the shear coefficient factor. The κ coefficient is a dimensionless quantity, dependent on the shape of the cross-section, which is introduced to account for the fact that the shear stress and strain are distributed not-uniformly over the cross-section [33]. In a linear elastic Timoshenko beam, the bending moment M_{xx} and the shear force Q_x are related to the angle of rotation φ and the displacement w by

$$M_{xx} = -E_sI\frac{\partial\varphi}{\partial x} \tag{9}$$

$$Q_x = \kappa AG_s(-\varphi + \frac{\partial w}{\partial x})$$

a) A cantilever beam with lateral displacement but with no rotation in the end (Figure 3a): Since the distributed load (force per length) $q(x)$ is zero, the solution to the first differential equation of Eq. (8) can be expressed as:

$$E_s I \frac{d^3\varphi}{dx^3} = q(x) = 0 \;\rightarrow E_s I \frac{d^2\varphi}{dx^2} = C_0 \;\rightarrow\; E_s I \frac{d\varphi}{dx} = C_0 x + C_1 \;\rightarrow E_s I \varphi = \frac{C_0}{2} x^2 + C_1 x + C_2 \tag{10}$$

By applying the boundary condition of no rotation at the root of the cantilever beam, Eq. (10) gives $C_2 = 0$. Similarly, applying the boundary condition of no rotation ($\varphi = 0$) at the end of the beam ($x = l$) to Eq. (10) gives $C_1 = -\frac{C_0 l}{2}$. Substituting C_1 and C_2 in the second line of Timoshenko beam theory (Eq. (8)) gives the deflection of the beam as follows:

$$w = \frac{C_0}{2E_s I}\left(\frac{x^3}{3} - l\frac{x^2}{2}\right) - \frac{E_s I}{\kappa A G_s}\frac{C_0}{2E_s I}(2x - l) + C_3 \tag{11}$$

The two other constants (C_0 , C_3) can be found from the boundary conditions in $x = 0$ and $x = l$. At the fixed end ($x = 0$), the deflection equals zero, hence:

$$C_3 = -\frac{C_0 l}{2\kappa A G_s} \tag{12}$$

Moreover, the deflection at the end of the beam equals δ which gives:

$$C_0 = \frac{-\delta}{\frac{l^3}{12E_s I} + \frac{l}{\kappa A G_s}} \tag{13}$$

By substituting C_0, C_1, C_2, C_3 in the first line of Eq. (8) and in Eq. (11), the Timoshenko beam theory for a cantilever beam with lateral displacement but with no rotation could be obtained as follows:

$$\begin{aligned} \varphi &= \frac{-\delta}{\frac{l^3}{6} + \frac{2E_s I l}{\kappa A G_s}}(x^2 - lx) \\ w &= \frac{-\delta}{\frac{l^3}{12E_s I} + \frac{l}{\kappa A G_s}}\left(\frac{1}{2E_s I}\left(\frac{x^3}{3} - l\frac{x^2}{2}\right) - \frac{1}{\kappa A G_s}x\right) \end{aligned} \tag{14}$$

Now it is possible to find the moments and forces shown in Figure 3a. As mentioned above, the bending moment M_{xx} and the shear force Q_x are related to the angle of rotation φ and the displacement w by Eq. (9). Therefore, by substituting $M = M_0$ and $Q_x = F$ at $x = l$ in respectively the first and second lines of Eq. (9), we have:

$$M_0 = \frac{\delta}{\frac{l^2}{6E_sI} + \frac{2}{\kappa AG_s}} \tag{15}$$

$$F = \frac{\delta}{\frac{l^3}{12E_sI} + \frac{l}{\kappa AG_s}}$$

b) A cantilever beam with rotation but with no lateral displacement in the end (Figure 3b): Since the distributed load $q(x)$ and the boundary condition of the beam at the clamped side ($x = 0$) for this case is similar to the previous case (Case a), the relationship for angle of rotation φ is the same as that given in Eq. (10), and also $C_2 = 0$. By considering $w = 0$ at both $x = 0$ and $x = l$, the constants C_1 and C_3 can be found through Eq. (11) as:

$$C_1 = C_0\left(\frac{2E_sI}{\kappa AG_sl} - \frac{l}{3}\right) \tag{16}$$

$$C_3 = \frac{C_1}{\kappa AG_s}$$

The beam at the free side ($x = l$) has a rotation with the known value of $\varphi = \theta$ which by substituting it in Eq. (10), we would have:

$$C_0 = \frac{\theta}{\frac{l^2}{6E_sI} + \frac{2}{\kappa AG_s}} \tag{17}$$

Therefore, the Timoshenko beam theory governing equations for a cantilever beam with rotation but with no lateral displacement at the end could be obtained:

$$\varphi = \frac{C_0x^2 + 2C_1x}{2E_sI} \tag{18}$$

$$w = \frac{1}{2E_sI}\left(\frac{C_0x^3}{3} + C_1x^2\right) - \frac{C_0}{\kappa AG_s}x$$

By considering $M_{xx} = M_0$ and $Q_x = F$ at $x = l$ in Eq. (9), the relationship of bending moment and shear force can be found as follows

$$M_0 = \left(\frac{\frac{2E_s I}{\kappa A G_s l} + \frac{2l}{3}}{\frac{l^2}{6E_s I} + \frac{2}{\kappa A G_s}} \right) \theta \tag{19}$$

$$F = \frac{\theta}{\frac{l^2}{6E_s I} + \frac{2}{\kappa A G_s}} \tag{20}$$

2.3. From Euler-Bernoulli to Timoshenko

The deformation of any arbitrary strut of an open-cell lattice structure can be decomposed into four basic deformations (Figure 1). According to relationships obtained for Euler-Bernoulli and Timoshenko beam theories in Sections 2.1 and 2.2, the resultant relationships for elastic modulus and Poisson's ratio of any structure based on Euler-Bernoulli theory can be converted into Timoshenko beam theory relationships by making the changes suggested in Table 1 into the stiffness matrix or in the derivation formulas. In the following, it is explained, how the changes have been made for each of the six unit cell types BCC, hexagonal packing, rhombicuboctahedron, diamond, truncated cube, and truncated octahedron (Figure 4-5) in order to convert their Euler-Bernoulli formulas [21, 24, 26, 27, 29, 34] to corresponding Timoshenko ones.

It must be noted that the commonly known geometries for the six noted unit cell shapes are presented in Figure 4 and the actual geometries used for both the analytical and numerical analyses are given in Figure 5. The reason for such conversion of unit cell shape for BCC is obvious as the molecular structure of BCC (Figure 4a) is composed of spheres rather than struts (Figure 5a). For the case of diamond, the unit cell shown in Figure 4b is rotated, and the unit cell in a specific direction (for which all the struts have similar angles with respect to horizontal plane) has been considered for analysis (Figure 5b). For the other cases, the unit cell conversion has been made in order to avoid neighbour cells having adjacent struts. If the neighbour cells share an edge, the analytical relationships obtained for unit cell does not represent that of a lattice structure. More explanation regarding this can be found in Section 2.1.2 of [27]. The conversion procedure from Euler-Bernoulli beam theory into Timoshenko beam theory for each unit cell is described as follows:

a) BCC

The relationships for elastic modulus and Poisson's ratio of BCC unit cell have been presented in equations "17" and "18" of [26]. In these equations, the axial extension ($\frac{AE_S}{l}$) and lateral bending ($\frac{12E_SI}{l^3}$) terms of Euler-Bernoulli theory can be identified easily. By substituting the term $\frac{12E_SI}{l^3}$ with $\left(\frac{1}{\frac{l^3}{12E_SI}+\frac{l}{\kappa AG_S}}\right)$, the relationships for elastic modulus and Poisson's ratio can be obtained.

b) Diamond

For transforming relationships of elastic modulus and Poisson's ratio from Euler-Bernoulli into Timoshenko beam theory, the basic equations "7" and "8" of [35] for elastic modulus and "29" and "30" of [35] for Poisson's ratio were considered. Axial extension ($\frac{AE_S}{l}$) and lateral bending ($\frac{12E_SI}{l^3}$) terms of Euler-Bernoulli theory can be identified easily. By substituting the term $\frac{12E_SI}{l^3}$ with $\left(\frac{1}{\frac{l^3}{12E_SI}+\frac{l}{\kappa AG_S}}\right)$, the relationships for elastic modulus and Poisson's ratio based on Timoshenko beam theory were obtained.

c) Hexagonal packing

For this unit cell, since the analytical relationships for mechanical properties of structure have not been derived based on Euler-Bernoulli theory in literature [29], the analytical relationships for Euler-Bernoulli and Timoshenko beam theories have been derived in this study. The detailed derivation can be found in Appendix C.

d) Rhombicuboctahedron

Since the final relationships for elastic modulus and Poisson's ratio of this unit cell have been presented in $\frac{r}{l}$ terms, and the stiffness matrix of unit cell contains $\frac{AE_S}{l}$, $\frac{12E_SI}{l^3}$, $\frac{G_SJ}{l}$ and $\frac{6E_SI}{l^2}$, recognition of terms provided in Table 1 in the final equations "29" and "33" of [36] is not possible. Therefore, by substituting the term $\frac{12E_SI}{l^3}$ with $\left(\frac{1}{\frac{l^3}{12E_SI}+\frac{l}{\kappa AG_S}}\right)$ and $\frac{6E_SI}{l^2}$ with $\left(\frac{1}{\frac{l^2}{6E_SI}+\frac{2}{\kappa AG_S}}\right)$ in the stiffness matrix (equation "27"of [36]) and solving the system of equations, the relationships based on Timoshenko theory were obtained.

e) Truncated cube

The procedure for truncated cube unit cell is very similar to what was described above for rhombicuboctahedron unit cell. The final stiffness matrix of unit cell in equation "36" of [37] contains $\frac{AE_S}{l}$ and $\frac{12E_SI}{l^3}$ terms. Therefore, by substituting the term $\frac{12E_SI}{l^3}$ with $\left(\frac{1}{\frac{l^3}{12E_SI}+\frac{l}{\kappa AG_S}}\right)$, the stiffness matrix based on Timoshenko beam theory can be derived. Afterwards, by solving the system of equations, the mechanical properties relationships based on Timoshenko beam theory were obtained.

f) Truncated octahedron

The relationships for elastic modulus and Poisson's ratio of truncated octahedron unit cell have been presented in equations "15" and "17" of [38]. Since the deformation of this unit cell includes axial extension and lateral bending, the terms $\frac{AE_S}{l}$ and $\frac{12E_SI}{l^3}$ can be extracted from these equations. By substitution the term $\frac{12EI}{l^3}$ with $\left(\frac{1}{\frac{l^3}{12E_SI}+\frac{l}{\kappa AG_S}}\right)$, the relationships presented for elastic modulus and Poisson's ratio can be transformed into corresponding Timoshenko ones.

It is worth noting that the relationships for normalized yield stress for 5 unit cells of six noted unit cells (BCC, hexagonal packing, rhombicuboctahedron, diamond, and truncated octahedron) based on Euler-Bernoulli and Timoshenko beam theories have been obtained separately in another study and could be found in [39].

2.4. Numerical analysis

The 3D CAD representation of the unit calls used for numerical modelling and analysis are demonstrated in Figure 5. The actual FE models of the unit cells along with the boundary conditions are demonstrated in Figure B in Appendix B. The struts of the unit cells were discretized using Timoshenko beam elements (element type 189 in ANSYS) and each strut was discretised using five beam elements. The beam elements were rigidly connected to each other at their shared vertices, and they were not allowed to rotate in any direction in the connecting point. The mechanical properties of the titanium alloy Ti-6Al-4V-ELI were used for modelling the local behaviour of the material in the FE models. A linear elastic material model with elastic modulus and Poisson's ratio of 113.8 GPa and 0.342 was implemented in the FE model. Since this type of element uses linear interpolation and takes transverse shear deformation into account, it is expected that the numerical results will be closer to the Timoshenko analytical solution. In the FE models of BCC, diamond, truncated cube, and truncated octahedron, a single unit cell with periodic boundary condition has been analysed under compressive loading (Figure Ba,b,e,f). For hexagonal packing and rhombicuboctahedron topologies, lattice structures consisting of $11\times11\times11$ unit cells was used for numerical modelling. This was due to the complexity of modelling the repetitive boundary conditions in these two unit cells, as in these two cases, each side of the unit cell is composed of two strut types (rather than one in the case of other unit cell types) which have non-symmetrical displacement under compressive loading (demonstrated as strut types A and B in Figure 5c-d).

In all the FE models, the lowermost nodes of the unit cell were fixed in the direction parallel to the loading direction and were not allowed to rotate in any direction. For the case of FE models made out of single unit cells (Figure B1a,b,e,f in Appendix B), the side vertices of the unit cell were constrained rotationally as they were shared with adjacent unit cells (repetitive boundary condition). In all the FE models, a downward displacement was applied to the uppermost node(s) of the single unit cell/lattice structure to induce axial deformation. The uppermost nodes were not allowed to rotate in any directions.

Mechanical properties of the FE models have been calculated based on basic definition of elastic modulus, Poisson's ratio, and yield stress:

- Elastic modulus: The formula $E_{UC} = \frac{F_{UC}L_{UC}}{A_{UC}\delta_{UC}}$ was used for calculating numerical elastic modulus, where L_{UC} is the structure length in the direction parallel to loading direction, A_{UC} is the cross-sectional area of the structure in the direction perpendicular to the loading direction, δ_{UC} is the downward displacement applied to the uppermost nodes, and F_{UC} is obtained by summing the reaction forces of the lowermost nodes.
- Poisson's ratio: The formula $\upsilon_{UC} = -\frac{\varepsilon_2}{\varepsilon_1} = -\frac{L_1\delta_2}{L_2\delta_1}$ was used for obtaining Poisson's ratio. In this formula, δ_1 and L_1 are the downward displacement applied to the uppermost nodes and unit cells length in the direction parallel to loading direction, respectively. Parameters δ_2 and L_2 are respectively the lateral displacement of the side nodes and the structure length in the direction perpendicular to loading direction.
- Yield stress: The formula $\frac{\sigma_y}{\sigma_{ys}} = \frac{F_{UC}}{A_{UC}\,\sigma_{max}}$ was used to calculate normalized yield stress. In this formula, F_{UC} is obtain from the sum of reaction forces of the lowermost nodes, A_{UC} is the structures cross-sectional area in the direction perpendicular to the loading direction, and σ_{max} is the maximum von Mises

stress experienced in the most critical point of the structure. The critical points of each unit cell can be seen in Figure 9.

For the cases which a lattice model was implemented for calculating numerical results of mechanical properties (rhombicuboctahedron and hexagonal packing), all the presented terms denoted by UC should be denoted by $Lattice$ and the lattice structures dimensions should be used for calculation.

3. Results

The transformed elastic modulus, Poisson's ratio, and yields stress relationships for the six geometries are presented in Table 2-4. For simplifying the equations, the terms $S = \frac{AE_S}{l}$, $T = \frac{1}{\frac{l^3}{12E_S I}+\frac{l}{\kappa AG_S}}$, $U = \frac{\frac{2E_S I}{\kappa AG_S l}+\frac{2l}{3}}{\frac{l^2}{6E_S I}+\frac{2}{\kappa AG_S}}$, $V = \frac{1}{\frac{l^2}{6E_S I}+\frac{2}{\kappa AG_S}}$, and $W = \frac{G_S J}{l}$ and have been used in the noted tables for the relationships based on the Timoshenko beam theory. For four of the geometries (BCC [26], rhombicuboctahedron [24], truncated cube [27], and truncated octahedron [34]), the original Euler-Bernoulli relationships have been presented in Table 2-3. In the case of hexagonal packing, the original Euler-Bernoulli relationships [29] for elastic modulus and Poisson's ratio have been improved and adjusted (the description on how and why can be found in Appendix C), and the improved relationships are presented in Table 2-3. For the case of diamond unit cell, the original relationships for elastic modulus and Poisson's ratio have been conserved but stated as a function of r/l rather than relative density, μ. As for the yield stress (Table 4), the analytical Euler-Bernoulli presented in our other paper [39] have been presented.

In order to compare the already-existing [21, 24, 26, 27, 29, 34] or improved Euler-Bernoulli analytical relationships with the newly transformed Timoshenko analytical relationships, the analytical relationships for both the Euler-Bernoulli and Timoshenko beam theory have been compared with numerical and experimental results in Figure 6-8. The relative density relationships for the six geometries are presented in Table 5.

For all the geometries, the newly transformed Timoshenko relationships have exceptionally good overlapping with the numerical results for all the mechanical properties: elastic modulus, Poisson's ratio, and yield stress (Figure 6-8). As for the previously obtained formulas obtained in the literature or newly adjusted Euler-Bernoulli formulas, the maximum difference between *Euler-Bernoulli* analytical elastic modulus and corresponding numerical values for BCC, diamond, Hexagonal packing, rhombicuboctahedron, truncated cube, and truncated octahedron (at relative density of $\mu = 0.5$) are respectively 21.34%, 57.71%, 20.21%, 14.52%, 14.98% and 45.54%. However, the corresponding difference between the *Timoshenko* analytical relationships and the numerical values for the noted geometries are respectively 1.13%, 2.21%, 8.29%, 2.97%, 0.43% and 3.15%.

Similarly, the maximum difference between *Euler-Bernoulli* analytical Poisson's ratio and corresponding numerical values for BCC, diamond, Hexagonal packing, rhombicuboctahedron, truncated cube, truncated octahedron are respectively 3.07%, 27.69%, 28.00%, 21.54%, 73.58% and 40.51%, while the corresponding difference between the *Timoshenko* analytical relationships and the numerical values for the noted geometries are respectively 0.133%, 0.826%, 0.899%, 6.24%, 1.36% and 0.498%, which shows a significant improvement in the accuracy of the analytical relationships. As it can be seen, the difference of the Timoshenko analytical and numerical values has improved significantly and to values around 1/10 of how much it was for the case of Euler-Bernoulli beam theories.

As for the yield stress (Figure 8), the analytical Euler-Bernoulli and Timoshenko relationships are identical for BCC and diamond. The reason is explained in Section 4.2. However, for the three other geometries, namely hexagonal packing, rhombicuboctahedron, and truncated octahedron, the analytical relationships based on

Euler-Bernoulli differ from the relationships obtained based on Timoshenko beam theory. Nevertheless, for all the cases, the Timoshenko analytical yield stress curve has exceptionally good agreement with numerical results (Figure 8). For BCC, diamond and truncated cube unit cells (the geometries which have the same yield stress analytical relationships for Euler-Bernoulli and Timoshenko beam theories), the maximum difference between analytical and numerical values is less than 0.25%. As for the three other geometries, the maximum difference between Euler-Bernoulli analytical normalized yield stress and corresponding numerical values for hexagonal packing, rhombicuboctahedron and truncated octahedron are respectively 21.25%. 3.02% and 7.52%. However, such differences for the analytical relationships based on Timoshenko beam theory and numerical values are respectively 9.49%, 0.09% and 0.162% which shows a significant improvement in the accuracy of the analytical relationships.

As for the proximity of the analytical/numerical elastic modulus and yield stress values to the experimental data, the experimental data points have been presented in Figure 6 and 8 for rhombicuboctahedron, truncated cube and diamond unit cells only, as in the literature, there is experimental measurements for such unit cells only [40]. As for the elastic modulus, converting the analytical relationships from Euler-Bernoulli to Timoshenko has led to closer proximity of analytical and experimental values (Figure 6b,d,e). As for the yield stress, for the three geometries for which experimental data points are available (diamond, rhombicuboctahedron, and truncated cube), the analytical relationships based on Euler-Bernoulli and Timoshenko are identical or almost overlapping, and both are in good agreement with experimental data points (Figure 8b,d,e).

4. Discussions

4.1. Why the new relationships give much better accuracy?

In this paper, new relationships based on Timoshenko beam theory have been derived for elastic modulus, Poisson's ratio, and yield strength of several lattice structures. In addition to considering of Timoshenko beam theories, some adjustments in deriving analytical relationships based on Euler-Bernoulli beam theory have been implemented for hexagonal packing unit cell (see Appendix C). Timoshenko beam theory takes into account shear deformation and rotational bending effects, making it suitable for describing the behaviour of thick beams. As a result, the new relationships based on Timoshenko beam theory give much better accuracy even at larger relative densities of lattice structures. This improvement is significant for analytical/experimental agreement and exceptional for analytical/numerical agreement. To give a more physically tangible understanding, it must be noted that taking into account the shear mechanisms of deformation effectively increases the flexibility of the beam which effectively leads to larger deflections of the struts (and therefore the whole lattice structure) under an imposed load. This leads to respectively lower and higher elastic modulus and Poisson's ratio of the structure for Timoshenko theory as compared to Euler-Bernoulli theory.

4.2. Yield strength

As mentioned in the Results section, the normalized yield stress relationships based on Timoshenko and Euler-Bernoulli theories are identical for BCC, diamond, and truncated cube structures and both theories have good agreement with the numerical results. However, for the hexagonal packing, truncated octahedron, and rhombicuboctahedron structures, the Euler-Bernoulli and Timoshenko yield strength results are quite different (particularly for hexagonal packing case) and the Timoshenko theory shows much better overlapping with numerical results as compared to how Euler-Bernoulli analytical curve does. The reason why the Timoshenko and Euler-Bernoulli yield strengths are identical for some geometries and different for some other is described extensively in [39], but it is explained here briefly. As introduced above, $T = \frac{12E_S I}{l^3}$, and $V = \frac{6E_S I}{l^2}$ for Euler-Bernoulli beam theory, and $T = \frac{1}{\frac{l^3}{12E_S I}+\frac{l}{\kappa A G_S}}$ and $V = \frac{1}{\frac{l^2}{6E_S I}+\frac{2}{\kappa A G_S}}$ for Timoshenko beam theory. For both the theories, $\frac{V}{T} = \frac{l}{2}$, hence as the analytical yield strength relationship for both the diamond and BCC in the final stage of derivation is a mere function of $\frac{V}{T}$, both the theories give the same result for yield strength relationship in these two unit cells. As for the truncated cube case, the normalized yield stress in critical strut could be obtained from forces and moments equilibrium and the strain causing the damage is merely due to axial loading rather than bending, hence the Euler-Bernoulli and Timoshenko theories give the same results. Nevertheless, for the three other unit cells, on the one hand, the displacement caused by bending needs to be taken into account in the calculations, and on the other hand, the formulas in the final stages of derivation are not a mere function of $\frac{V}{T}$, and the V and T terms are present independently and not in a fraction form in such a way that one is a factor of the other. Therefore, the results differ for Euler-Bernoulli and Timoshenko theories for the three other unit cells.

4.3. Some points regarding experimental data points

Both analytical and numerical techniques over-predict the experimental elastic modulus of the diamond and truncated cube porous structures, while they under-predict their experimental yield stress. The random irregularities and imperfections created during the AM process diminish the elastic modulus of the lattice structures. These defects create weak links in the structure that lower the mechanical properties of structures. On the other hand, in the case of yield stress, when the initial regions of the lattice structures in the critical points (which experience the highest stress levels in the whole lattice structure) are yielded, their local yield stress increases due to strain-hardening phenomenon, and the structure is still able to remain almost intact as the strain-hardening strengthens the structure at the initial damage points. However, when the external load is increased even further, the second (and possibly the third) critical points are damaged and together with the initial points, the structure is unable to keep its integrity as it was before, as now damage and softening has propagated throughout the whole structure. That is why in practice, the yielding in the structure as a whole usually occurs for the external loads which are between the external loads which theoretically cause the first and second set of critical points become locally yielded. This was shown in [31].

4.4. Application to biomedical implants

There are several applications for cellular materials including heat exchangers, filters, load bearing components, and biomedical implants. Lattice structures can improve the implants' performance significantly, from both mechanical and biological points of view. Obtaining the accurate characteristics and mechanical properties of the lattice structures are necessary to improve their use in orthopaedic implants. The mechanical properties of lattice structures depend mainly on the following three parameters: the material they are made of, the cell topology, and the relative density. Obtaining accurate analytical relationships for different cell topologies is a crucial factor in developing computational tools for designing patient-specific implants with non-uniform mechanical property distribution. In this paper, we presented a new and convenient method to transform properties of a lattice structure from Euler-Bernoulli theory into Timoshenko theory for both the already-existing Euler-Bernoulli relationships and for future studies. Using the transformation relationships presented in this paper (Table 1), developing new analytical relationships based on Timoshenko beam theory becomes easier than how it has been before.

5. Conclusions

In this paper, a new methodology to convert analytical relationships based on Euler-Bernoulli to Timoshenko has been presented. Six unit cells for which Euler-Bernoulli analytical relationships could be found in the literature, but Timoshenko theories could not be found have been considered: BCC, hexagonal packing, rhombicuboctahedron, diamond, truncated cube, and truncated octahedron [21, 24, 26, 27, 29, 34]. The results of this study demonstrated that converting analytical relationships based on Euler-Bernoulli to equivalent Timoshenko ones can decrease the difference between the analytical and numerical values for one order of magnitude which is a significant improvement in accuracy of the analytical formulas. The methodology presented in this study is not only beneficial to the already-existing analytical relationships but also to facilitate derivation of analytical relationships for other, yet unexplored, unit cell types.

REFERENCES

1. Pałka, K. and R. Pokrowiecki, *Porous Titanium implants: A review.* Advanced Engineering Materials, 2018. **20**(5): p. 1700648.
2. Hedayati, R. and M. Sadighi, *Low-velocity impact behaviour of open-cell foams.* Journal of Theoretical and Applied Mechanics, 2018. **56**.
3. Torres, Y., J. Pavón, and J. Rodríguez, *Processing and characterization of porous titanium for implants by using NaCl as space holder.* Journal of Materials Processing Technology, 2012. **212**(5): p. 1061-1069.
4. Hedayati, R., M. Sadighi, M. Mohammadi-Aghdam, and H. Hosseini-Toudeshky, *Comparison of elastic properties of open-cell metallic biomaterials with different unit cell types.* Journal of Biomedical Materials Research Part B: Applied Biomaterials, 2017.
5. Brandl, E., U. Heckenberger, V. Holzinger, and D. Buchbinder, *Additive manufactured AlSi10Mg samples using Selective Laser Melting (SLM): Microstructure, high cycle fatigue, and fracture behavior.* Materials & Design, 2012. **34**: p. 159-169.
6. Hedayati, R., S.A. Yavari, and A. Zadpoor, *Fatigue crack propagation in additively manufactured porous biomaterials.* Materials Science and Engineering: C, 2017. **76**: p. 457-463.
7. Balla, V.K., S. Bodhak, S. Bose, and A. Bandyopadhyay, *Porous tantalum structures for bone implants: fabrication, mechanical and in vitro biological properties.* Acta biomaterialia, 2010. **6**(8): p. 3349-3359.
8. Kerckhofs, G., G. Pyka, M. Moesen, S. Van Bael, J. Schrooten, and M. Wevers, *High-resolution microfocus X-ray computed tomography for 3D surface roughness measurements of additive manufactured porous materials.* Advanced Engineering Materials, 2013. **15**(3): p. 153-158.
9. Sumner, D.R. and J.O. Galante, *Determinants of stress shielding.* Clin. Orthop. Relat. Res, 1991. **274**: p. 202-212.
10. Li, G., L. Wang, W. Pan, F. Yang, W. Jiang, X. Wu, X. Kong, K. Dai, and Y. Hao, *In vitro and in vivo study of additive manufactured porous Ti6Al4V scaffolds for repairing bone defects.* Scientific reports, 2016. **6**: p. 34072.
11. Taniguchi, N., S. Fujibayashi, M. Takemoto, K. Sasaki, B. Otsuki, T. Nakamura, T. Matsushita, T. Kokubo, and S. Matsuda, *Effect of pore size on bone ingrowth into porous titanium implants fabricated by additive manufacturing: an in vivo experiment.* Materials Science and Engineering: C, 2016. **59**: p. 690-701.
12. Epasto, G., G. Palomba, D. D'Andrea, E. Guglielmino, S. Di Bella, and F. Traina, *Ti-6Al-4V ELI microlattice structures manufactured by electron beam melting: Effect of unit cell*

dimensions and morphology on mechanical behaviour. Materials Science and Engineering: A, 2019. **753**: p. 31-41.

13. Xiao, L., W. Song, C. Wang, H. Liu, H. Tang, and J. Wang, *Mechanical behavior of open-cell rhombic dodecahedron Ti–6Al–4V lattice structure.* Materials Science and Engineering: A, 2015. **640**: p. 375-384.
14. Hedayati, R., M. Mirzaali, L. Vergani, and A. Zadpoor, *Action-at-a-distance metamaterials: Distributed local actuation through far-field global forces.* APL Materials, 2018. **6**(3): p. 036101.
15. Gonzalez, F.J.Q. and N. Nuno, *Finite element modeling of manufacturing irregularities of porous materials.* Biomater. Biomech. Bioeng, 2016. **3**(1): p. 1-14.
16. Jahadakbar, A., N. Shayesteh Moghaddam, A. Amerinatanzi, D. Dean, H. Karaca, and M. Elahinia, *Finite element simulation and additive manufacturing of stiffness-matched niti fixation hardware for mandibular reconstruction surgery.* Bioengineering, 2016. **3**(4): p. 36.
17. Mahmoud, D. and M.A. Elbestawi, *Lattice structures and functionally graded materials applications in additive manufacturing of orthopedic implants: a review.* Journal of Manufacturing and Materials Processing, 2017. **1**(2): p. 13.
18. Hedayati, R., H. Hosseini-Toudeshky, M. Sadighi, M. Mohammadi-Aghdam, and A. Zadpoor, *Multiscale modeling of fatigue crack propagation in additively manufactured porous biomaterials.* International Journal of Fatigue, 2018. **113**: p. 416-427.
19. Badiche, X., S. Forest, T. Guibert, Y. Bienvenu, J.-D. Bartout, P. Ienny, M. Croset, and H. Bernet, *Mechanical properties and non-homogeneous deformation of open-cell nickel foams: application of the mechanics of cellular solids and of porous materials.* Materials Science and Engineering: A, 2000. **289**(1-2): p. 276-288.
20. Geng, X., L. Ma, C. Liu, C. Zhao, and Z. Yue, *A FEM study on mechanical behavior of cellular lattice materials based on combined elements.* Materials Science and Engineering: A, 2018. **712**: p. 188-198.
21. Ahmadi, S., G. Campoli, S.A. Yavari, B. Sajadi, R. Wauthlé, J. Schrooten, H. Weinans, and A. Zadpoor, *Mechanical behavior of regular open-cell porous biomaterials made of diamond lattice unit cells.* Journal of the mechanical behavior of biomedical materials, 2014. **34**: p. 106-115.
22. Hedayati, R., M. Sadighi, M. Mohammadi-Aghdam, and A. Zadpoor, *Analytical relationships for the mechanical properties of additively manufactured porous biomaterials based on octahedral unit cells.* Applied Mathematical Modelling, 2017.
23. Babaee, S., B.H. Jahromi, A. Ajdari, H. Nayeb-Hashemi, and A. Vaziri, *Mechanical properties of open-cell rhombic dodecahedron cellular structures.* Acta Materialia, 2012. **60**(6): p. 2873-2885.
24. Hedayati, R., M. Sadighi, M. Mohammadi-Aghdam, and A. Zadpoor, *Mechanics of additively manufactured porous biomaterials based on the rhombicuboctahedron unit cell.* Journal of the mechanical behavior of biomedical materials, 2016. **53**: p. 272-294.
25. Ghavidelnia, N., R. Hedayati, M. Sadighi, and M. Mohammadi-Aghdam, *Development of porous implants with non-uniform mechanical properties distribution based on CT images.* Applied Mathematical Modelling, 2020.
26. Ptochos, E. and G. Labeas, *Elastic modulus and Poisson's ratio determination of micro-lattice cellular structures by analytical, numerical and homogenisation methods.* Journal of Sandwich Structures & Materials, 2012. **14**(5): p. 597-626.
27. Hedayati, R., M. Sadighi, M. Mohammadi-Aghdam, and A. Zadpoor, *Mechanical properties of regular porous biomaterials made from truncated cube repeating unit cells: Analytical solutions and computational models.* Materials Science and Engineering: C, 2016. **60**: p. 163-183.
28. Karaji, Z.G., R. Hedayati, B. Pouran, I. Apachitei, and A.A. Zadpoor, *Effects of plasma electrolytic oxidation process on the mechanical properties of additively manufactured porous biomaterials.* Materials Science and Engineering: C, 2017. **76**: p. 406-416.
29. Ko, W., *Deformations of foamed elastomers.* Journal of Cellular Plastics, 1965. **1**(1): p. 45-50.

30. Gibson, L.J. and M.F. Ashby, *Cellular solids: structure and properties*. 1999: Cambridge university press.
31. Hedayati, R., M. Sadighi, M. Mohammadi-Aghdam, and A. Zadpoor, *Mechanical behavior of additively manufactured porous biomaterials made from truncated cuboctahedron unit cells*. International Journal of Mechanical Sciences, 2016. **106**: p. 19-38.
32. Dementjev, A. and O. Tarakanov, *Influence of the cellular structure of foams on their mechanical properties*. Mech Polym, 1970. **4**: p. 594-602.
33. Cowper, G. *The shear coefficient in Timoshenko's beam theory*. 1966. ASME.
34. Zhu, H., J. Knott, and N. Mills, *Analysis of the elastic properties of open-cell foams with tetrakaidecahedral cells*. Journal of the Mechanics and Physics of Solids, 1997. **45**(3): p. 319327-325343.
35. Ahmadi, S., G. Campoli, S.A. Yavari, B. Sajadi, R. Wauthlé, J. Schrooten, H. Weinans, and A.J.J.o.t.m.b.o.b.m. Zadpoor, *Mechanical behavior of regular open-cell porous biomaterials made of diamond lattice unit cells*. 2014. **34**: p. 106-115.
36. Hedayati, R., M. Sadighi, M. Mohammadi-Aghdam, and A.J.J.o.t.m.b.o.b.m. Zadpoor, *Mechanics of additively manufactured porous biomaterials based on the rhombicuboctahedron unit cell*. 2016. **53**: p. 272-294.
37. Hedayati, R., M. Sadighi, M. Mohammadi-Aghdam, A. Zadpoor, and E. C, *Mechanical properties of regular porous biomaterials made from truncated cube repeating unit cells: Analytical solutions and computational models*. Materials Science Engineering: A, 2016. **60**: p. 163-183.
38. Zhu, H., J. Knott, N.J.J.o.t.M. Mills, and P.o. Solids, *Analysis of the elastic properties of open-cell foams with tetrakaidecahedral cells*. 1997. **45**(3): p. 319-343.
39. Ghavidelnia, N., S. Jedari Salami, and R. Hedayati, *Analytical relationships for yield stress of five mechanical meta-biomaterials*. Mechanics Based Design of Structures and Machines, 2020: p. 1-23.
40. Ahmadi, S.M., S.A. Yavari, R. Wauthle, B. Pouran, J. Schrooten, H. Weinans, and A.A. Zadpoor, *Additively manufactured open-cell porous biomaterials made from six different space-filling unit cells: The mechanical and morphological properties*. Materials, 2015. **8**(4): p. 1871-1896.

Figure Captions

Figure 1- **General deformation of a cantilever beam with axial and lateral displacements as well as flexural and torsional rotations in the free end**

Figure 2- **Forces and moments required to cause (a) lateral displacement δ with no rotation at the free end of the beam, and (b) rotation θ with no lateral displacement at the free end of the beam, (c) pure axial extension, and (d) pure twist in the free end of an Euler-Bernoulli beam [31, 39]**

Figure 3- **Forces and moments required to cause (a) lateral displacement δ with no rotation at the free end of the beam, and (b) rotation θ with no lateral displacement at the free end of the beam, (c) pure axial extension, and (d) pure twist in the free end of a Timoshenko beam**

Figure 4- **Unit cells of (a) BCC, (b) Diamond, (c) Hexagonal packing, (d) Rhombicuboctahedron, (e) Truncated cube, and (f) Truncated octahedron.**

Figure 5- **Unit cells used for analytical and numerical analysis: (a) BCC, (b) Diamond, (c) Hexagonal packing, (d) Rhombicuboctahedron, (e) Truncated cube, and (f) Truncated octahedron.**

Figure 6- **Comparison of analytical (Euler-Bernoulli and Timoshenko) and numerical values of normalized Elastic modulus for different unit cells: (a) BCC, (b) Diamond, (c) Hexagonal packing, (d) Rhombicuboctahedron, (e) Truncated cube, and (f) Truncated octahedron.**

Figure 7- **Comparison of analytical (Euler-Bernoulli and Timoshenko) and numerical values of Poisson's ratio for different unit cells: (a) BCC, (b) Diamond, (c) Hexagonal packing, (d) Rhombicuboctahedron, (e) Truncated cube, and (f) Truncated octahedron.**

Figure 8- **Comparison of analytical (Euler-Bernoulli and Timoshenko) and numerical values of Yield stress for different unit cells: (a) BCC, (b) Diamond, (c) Hexagonal packing, (d) Rhombicuboctahedron, (e) Truncated cube, and (f) Truncated octahedron.**

Figure 9- **unit cells stress contour: (a) BCC, (b) Diamond, (c) Hexagonal packing, (d) Rhombicuboctahedron, (e) Truncated cube, and (f) Truncated octahedron.**

Table Captions

Table 1: Conversion table for converting mechanical properties relationships based on Euler-Bernoulli beam theory to mechanical properties relationships based on Timoshenko beam theory

Table 2: Normalized elastic modulus relationships based on Euler-Bernoulli and Timoshenko beam theories for different unit cells ($S = \frac{AE_s}{l}$, $T = \frac{1}{\frac{l^3}{12E_sI}+\frac{l}{\kappa AG_s}}$, $V = \frac{1}{\frac{l^2}{6E_sI}+\frac{2}{\kappa AG_s}}$, **and** $W = \frac{G_sJ}{l}$)

Table 3: Poisson's ratio relationships based on Euler-Bernoulli and Timoshenko beam theories for different unit cell geometries ($S = \frac{AE_s}{l}$, $T = \frac{1}{\frac{l^3}{12E_sI}+\frac{l}{\kappa AG_s}}$, $V = \frac{1}{\frac{l^2}{6E_sI}+\frac{2}{\kappa AG_s}}$, $W = \frac{G_sJ}{l}$)

Table 4: Relative yield stress relationships based on Euler-Bernoulli and Timoshenko beam theories for different unit cells ($S = \frac{AE_s}{l}$, $= \frac{1}{\frac{l^3}{12E_sI}+\frac{l}{\kappa AG_s}}$, $U = \frac{\frac{2E_sI}{\kappa AGl}+\frac{2l}{3}}{\frac{l^2}{6E_sI}+\frac{2}{\kappa AG_s}}$, $V = \frac{1}{\frac{l^2}{6E_sI}+\frac{2}{\kappa AG_s}}$, **and** $W = \frac{G_sJ}{l}$)

Table 5: Relative density relationships for different unit cells

Tables

Table 1: Conversion table for converting mechanical properties relationships based on Euler-Bernoulli beam theory to mechanical properties relationships based on Timoshenko beam theory

Term	Euler Bernoulli Theory	→	Timoshenko Theory
Axial Tension/Compression	$\left(\frac{AE_s}{l}\right)u$	→	$\left(\frac{AE_s}{l}\right)u$
Torsion	$\left(\frac{G_sJ}{l}\right)\varphi$	→	$\left(\frac{G_sJ}{l}\right)\varphi$
Lateral deformation Force	$\left(\frac{12E_sI}{l^3}\right)v$	→	$\left(\frac{1}{\frac{l^3}{12E_sI}+\frac{l}{\kappa AG_s}}\right)v$
Lateral deformation Moment	$\left(\frac{6E_sI}{l^2}\right)v$	→	$\left(\frac{1}{\frac{l^2}{6E_sI}+\frac{2}{\kappa AG_s}}\right)v$
Rotation Force	$\left(\frac{6E_sI}{l^2}\right)\theta$	→	$\left(\frac{1}{\frac{l^2}{6E_sI}+\frac{2}{\kappa AG_s}}\right)\theta$
Rotation Moment	$\left(\frac{4E_sI}{l}\right)\theta$	→	$\left(\frac{\frac{2E_sI}{\kappa AG_sl}+\frac{2l}{3}}{\frac{l^2}{6E_sI}+\frac{2}{\kappa AG_s}}\right)\theta$

Table 2: Normalized elastic modulus relationships based on Euler-Bernoulli and Timoshenko beam theories for different unit cells ($\boldsymbol{S = \frac{AE_s}{l}}$, $\boldsymbol{T = \frac{1}{\frac{l^3}{12E_sI}+\frac{l}{\kappa AG_s}}}$, $\boldsymbol{V = \frac{1}{\frac{l^2}{6E_sI}+\frac{2}{\kappa AG_s}}}$, and $\boldsymbol{W = \frac{G_sJ}{l}}$)

Unit cell	**Relative elastic modulus, E/E_s**	
	Euler-Bernoulli theory	Timoshenko theory
BCC	$\frac{4\sqrt{3}}{\left(\frac{l^2}{\pi r^2}+\frac{l^4}{2\pi r^4}\right)}$ [26]	$\frac{4\sqrt{3}}{E\left(\frac{4l}{3S}+\frac{8l}{3T}\right)}$
Diamond	$\frac{3\sqrt{3}}{\frac{8}{3\pi}\left(\frac{l}{r}\right)^4+\frac{4}{\pi}\left(\frac{l}{r}\right)^2}$ [21]	$\frac{3\sqrt{3}}{E\left(\frac{8l}{T}+\frac{4l}{S}\right)}$
Hexagonal packing	$\frac{\pi\sqrt{3}}{4}\left(\frac{r}{l}\right)^2\left(1+\frac{1}{\frac{5}{9}+\frac{4}{27}\left(\frac{l}{r}\right)^2}\right)$ (see Appendix C)	$\frac{\sqrt{3}S\left(1+\frac{1}{\frac{5}{9}+\frac{4S}{9T}}\right)}{4El}$
Rhombicuboctahedron	$\frac{4\pi\left(\frac{r}{l}\right)^2}{3(1+\sqrt{2})}\left[\frac{4+108\left(\frac{r}{l}\right)^2+207\left(\frac{r}{l}\right)^4+81\left(\frac{r}{l}\right)^6+\frac{G}{E}\left(\frac{2}{3}+19\left(\frac{r}{l}\right)^2+45\left(\frac{r}{l}\right)^4+18\left(\frac{r}{l}\right)^6\right)}{8+70\left(\frac{r}{l}\right)^2+105\left(\frac{r}{l}\right)^4+27\left(\frac{r}{l}\right)^6+\frac{G}{E}\left(\frac{4}{3}+13\left(\frac{r}{l}\right)^2+23\left(\frac{r}{l}\right)^4+6\left(\frac{r}{l}\right)^6\right)}\right]$ [24]	$\frac{4S(2WS^3+19WS^2T+15WST^2+2WT^3+4S^3V+36S^2TV+23ST^2V+3T^3V)\mathrm{L}_{UC}}{E(12WS^3+39WS^2T+23WST^2+2WT^3+24S^3V+70S^2TV+35ST^2V+3T^3V)\mathrm{A}_{UC}}$
Truncated cube	$\frac{2\pi}{\sqrt{2}+1}\left(\frac{r}{l}\right)^2\frac{1+9\left(\frac{r}{l}\right)^2}{5+21\left(\frac{r}{l}\right)^2}$ [27]	$\frac{8S(S+3T)\mathrm{L}_{UC}}{E(5S+7T)\mathrm{A}_{UC}}$
Truncated octahedron	$\frac{6\sqrt{2}I}{l^4\left(1+\frac{12I}{Al^2}\right)}$ [34]	$\frac{1}{\sqrt{2}El\left(\frac{1}{S}+\frac{1}{T}\right)}$

Table 3: Poisson's ratio relationships based on Euler-Bernoulli and Timoshenko beam theories for different unit cell geometries ($S = \frac{AE_S}{l}$, $T = \frac{1}{\frac{l^3}{12E_S I} + \frac{l}{\kappa A G_S}}$, $V = \frac{1}{\frac{l^2}{6E_S I} + \frac{2}{\kappa A G_S}}$, $W = \frac{G_S J}{l}$)

Unit cell	**Poisson's ratio, $\boldsymbol{v}$**	
	Euler-Bernoulli theory	Timoshenko theory
BCC	$\dfrac{-\frac{1}{\pi r^2} + \frac{l^2}{4\pi r^4}}{\frac{1}{\pi r^2} + \frac{l^2}{2\pi r^4}}$ [26]	$\dfrac{-\frac{1}{S} + \frac{1}{T}}{\frac{1}{S} + \frac{2}{T}}$
Diamond	$\dfrac{1 - 3\left(\frac{r}{l}\right)^2}{2 - 3\left(\frac{r}{l}\right)^2}$ [21]	$\dfrac{-\frac{1}{S} + \frac{1}{T}}{\frac{1}{S} + \frac{2}{T}}$
Hexagonal packing	$\dfrac{-\frac{1}{9} + \frac{1}{27}\left(\frac{l}{r}\right)^2}{\frac{5}{9} + \frac{4}{27}\left(\frac{l}{r}\right)^2}$ (see Appendix C)	$\dfrac{\frac{S}{T} - 1}{5 + \frac{4S}{T}}$
Rhombicuboctahedron	$\frac{1}{3}\left[\dfrac{8 - 12\left(\frac{r}{l}\right)^2 - 36\left(\frac{r}{l}\right)^4 + \frac{G}{E}\left(\frac{4}{3} - \left(\frac{r}{l}\right)^2 - 9\left(\frac{r}{l}\right)^4\right)}{8 + 70\left(\frac{r}{l}\right)^2 + 105\left(\frac{r}{l}\right)^4 + 27\left(\frac{r}{l}\right)^6 + \frac{G}{E}\left(\frac{4}{3} + 13\left(\frac{r}{l}\right)^2 + 23\left(\frac{r}{l}\right)^4 + 6\left(\frac{r}{l}\right)^6\right)}\right]$ [24]	$\dfrac{S(S-T)(4WS + 3WT + 8SV + 4TV)}{12WS^3 + 39WS^2T + 23WST^2 + 2WT^3 + 24S^3V + 70S^2TV + 35ST^2V + 3T^3V}$
Truncated cube	$\dfrac{1 - 3\left(\frac{r}{l}\right)^2}{5 + 21\left(\frac{r}{l}\right)^2}$ [27]	$\dfrac{\frac{1}{T} - \frac{1}{S}}{\frac{5}{T} + \frac{7}{S}}$
Truncated octahedron	$0.5\dfrac{Al^2 - 12I}{Al^2 + 12I}$ [34]	$\dfrac{1}{2}\dfrac{S - T}{S + T}$

Table 4: Relative yield stress relationships based on Euler-Bernoulli and Timoshenko beam theories for different unit cells ($\boldsymbol{S = \frac{AE_s}{l}}$, $\boldsymbol{= \frac{1}{\frac{l^3}{12E_sI}+\frac{l}{\kappa AG_s}}}$, $\boldsymbol{U = \frac{\frac{2E_sI}{\kappa AGl}+\frac{2l}{3}}{\frac{l^2}{6E_sI}+\frac{2}{\kappa AG_s}}}$, $\boldsymbol{V = \frac{1}{\frac{l^2}{6E_sI}+\frac{2}{\kappa AG_s}}}$, and $\boldsymbol{W = \frac{G_sJ}{l}}$)

Unit cell	**Relative yield stress, $\frac{\sigma_y}{\sigma_{ys}}$**		
	Euler-Bernoulli theory		Timoshenko theory
BCC	$\frac{1}{\frac{1}{3\pi\sqrt{3}}\left(\frac{l}{r}\right)^2+\frac{4}{\pi\sqrt{6}}\left(\frac{l}{r}\right)^3}$	[39]	$\frac{3\sqrt{3}}{l^2(\frac{1}{A}+\frac{cl}{\sqrt{2}I})}$
Diamond	$\frac{1}{\frac{4}{3\pi\sqrt{3}}\left(\frac{l}{r}\right)^2+\frac{8\sqrt{2}}{\pi\sqrt{3}}\left(\frac{l}{r}\right)^3}$	[39]	$\frac{3\sqrt{3}}{4l^2(\frac{1}{A}+\frac{cl}{\sqrt{2}I})}$
Hexagonal packing	$\frac{\pi\sqrt{3}}{4}\left(\frac{r}{l}\right)^2\left(1+\frac{1}{\frac{5}{9}+\frac{4}{27}\left(\frac{l}{r}\right)^2}\right)$	[39]	$\frac{\sqrt{3}S\left(1+\frac{1}{\frac{5}{9}+\frac{4S}{9T}}\right)}{4El}$
Rhombicuboctahedron	$\frac{4A}{\mathrm{A}_{UC}}\left(1-\frac{6\sqrt{2}(A^2l^4-6\mathrm{AI}l^2-72\mathrm{I}^2)rAl}{1728\left(4.5+\frac{G_s}{E_s}\right)\mathrm{I}^3+1080\left(4.6+\frac{G_s}{E_s}\right)A\mathrm{I}^2l^2+6\left(108+19\frac{G_s}{E_s}\right)A^2\mathrm{I}l^4+\left(6+\frac{G_s}{E_s}\right)A^3l^6+6\sqrt{2}(A^2l^4-6\mathrm{AI}l^2-72\mathrm{I}^2)rAl}\right)$		* (See the footnote of the table)
Truncated cube	$\frac{\pi}{\left(\sqrt{2}+1\right)^2}\left(\frac{r}{l}\right)^2$	[4]	$\frac{A}{l^2\left(\sqrt{2}+1\right)^2}$
Truncated octahedron	$\frac{1}{\frac{\sqrt{2}}{2\pi}\left(\frac{l}{r}\right)^2+\frac{\sqrt{2}}{\pi}\left(\frac{l}{r}\right)^3}$	[39]	$\frac{\sqrt{2}}{l^2\left(\frac{Vc\left(\frac{3}{T}+\frac{1}{S}\right)}{I}+\frac{S\left(\frac{1}{T}+\frac{3}{S}\right)}{A}\right)}$

* The Timoshenko-based relationship for the yield stress of rhombicuboctahedron is:

$$\frac{16IA}{\mathrm{A}_{UC}}\left(\frac{2\acute{W}\left(\acute{S}^3+\acute{T}^3\right)+19\acute{W}\acute{S}^2\acute{T}+15\acute{W}\acute{S}\acute{T}^2+4\acute{S}^3\acute{V}+36\acute{S}^2\acute{T}\acute{V}+23\acute{S}\acute{T}^2V+3\acute{T}^3\acute{V}}{2I\left(2\acute{W}\acute{S}^3+2\acute{W}\acute{T}^3+19\acute{W}\acute{S}^2\acute{T}+15\acute{W}\acute{S}\acute{T}^2+4\acute{S}^3\acute{V}+36\acute{S}^2\acute{T}\acute{V}+23\acute{S}\acute{T}^2\acute{V}+3\acute{T}^3\acute{V}\right)+\sqrt{2}rA\left(8\acute{S}^2\acute{U}\acute{V}-4\acute{S}\acute{T}\acute{U}\acute{V}-4\acute{T}^2\acute{U}\acute{V}-2\acute{S}^2\acute{V}^2+\acute{S}\acute{T}\acute{V}^2+\acute{T}^2\acute{V}^2\right)}\right)$$

where

$\boldsymbol{\acute{S} = \frac{2AE_s}{l}}$, $\boldsymbol{\acute{T} = \frac{1}{\frac{l^3}{96E_sI}+\frac{l}{\kappa AG_s}}}$, $\boldsymbol{\acute{U} = \frac{\frac{4E_sI}{\kappa AG_sl}+\frac{l}{3}}{\frac{l^2}{24E_sI}+\frac{2}{\kappa AG_s}}}$, $\boldsymbol{\acute{V} = \frac{1}{\frac{l^2}{24E_sI}+\frac{2}{\kappa AG_s}}}$, $\boldsymbol{\acute{W} = \frac{2G_sJ}{l}}$

Table 5: Relative density relationships for different unit cells

Unit cell	μ, Relative density
BCC	$3\sqrt{3}\pi\left(\frac{r}{l}\right)^2 - 4\sqrt{6}\pi\left(\frac{r}{l}\right)^3$ [39]
Diamond	$\frac{3\sqrt{3}\pi}{4}\left(\frac{r}{l}\right)^2 - \frac{9\sqrt{2}}{4}\left(\frac{r}{l}\right)^3$
Hexagonal packing	$\frac{5\pi}{2\sqrt{3}}\left(\frac{r}{l}\right)^2$
Rhombicuboctahedron	$\frac{36\pi}{7+\sqrt{5}}\left(\frac{r}{l}\right)^2 - \frac{12(12.0404)}{7+\sqrt{5}}\left(\frac{r}{l}\right)^3$ [24]
Truncated cube	$\frac{15\pi}{\left(1+\sqrt{3}\right)^3}\left(\frac{r}{l}\right)^2$ [27]
Truncated octahedron	$\frac{3\pi}{2\sqrt{2}}\left(\frac{r}{l}\right)^2$ [38]

FIGURES

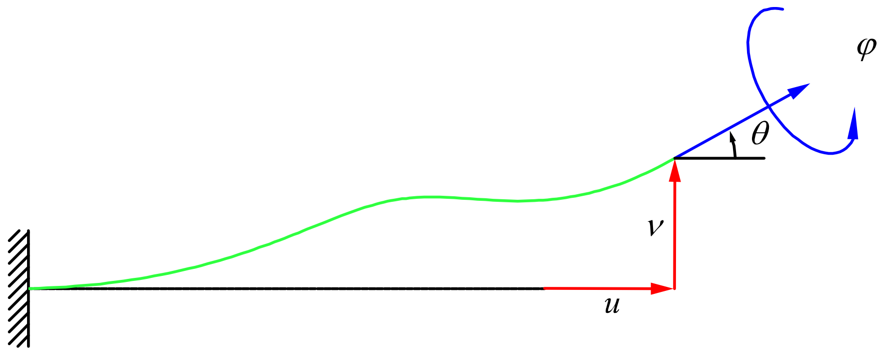

Figure 1- General deformation of a cantilever beam with axial and lateral displacements as well as flexural and torsional rotations in the free end

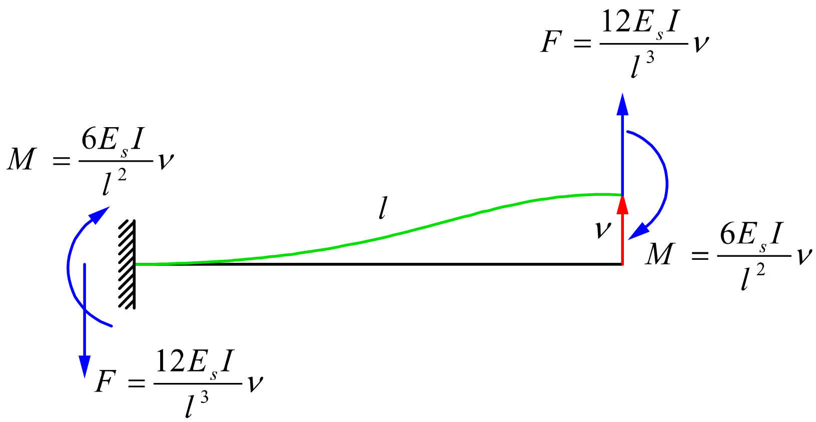

(a)

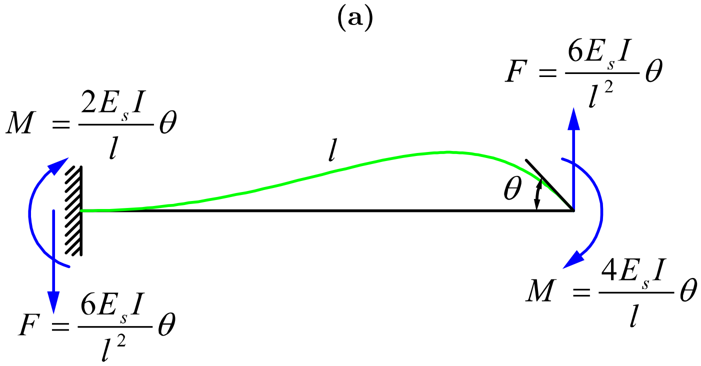

(b)

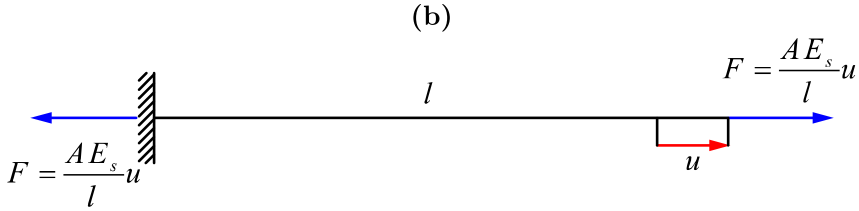

(c)

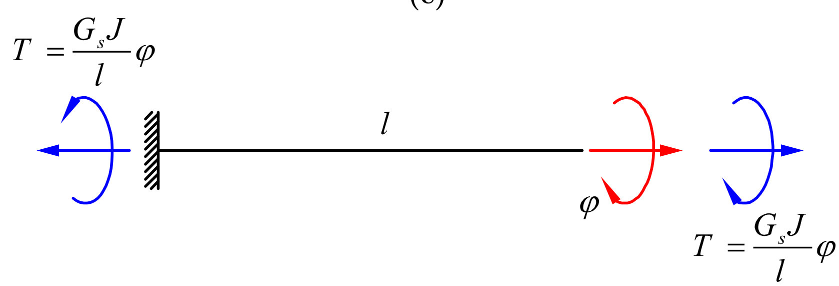

(d)

Figure 2- Forces and moments required to cause (a) lateral displacement $\boldsymbol{\delta}$ with no rotation at the free end of the beam, and (b) rotation $\boldsymbol{\theta}$ with no lateral displacement at the free end of the beam, (c) pure axial extension, and (d) pure twist in the free end of an Euler-Bernoulli beam [31, 39]

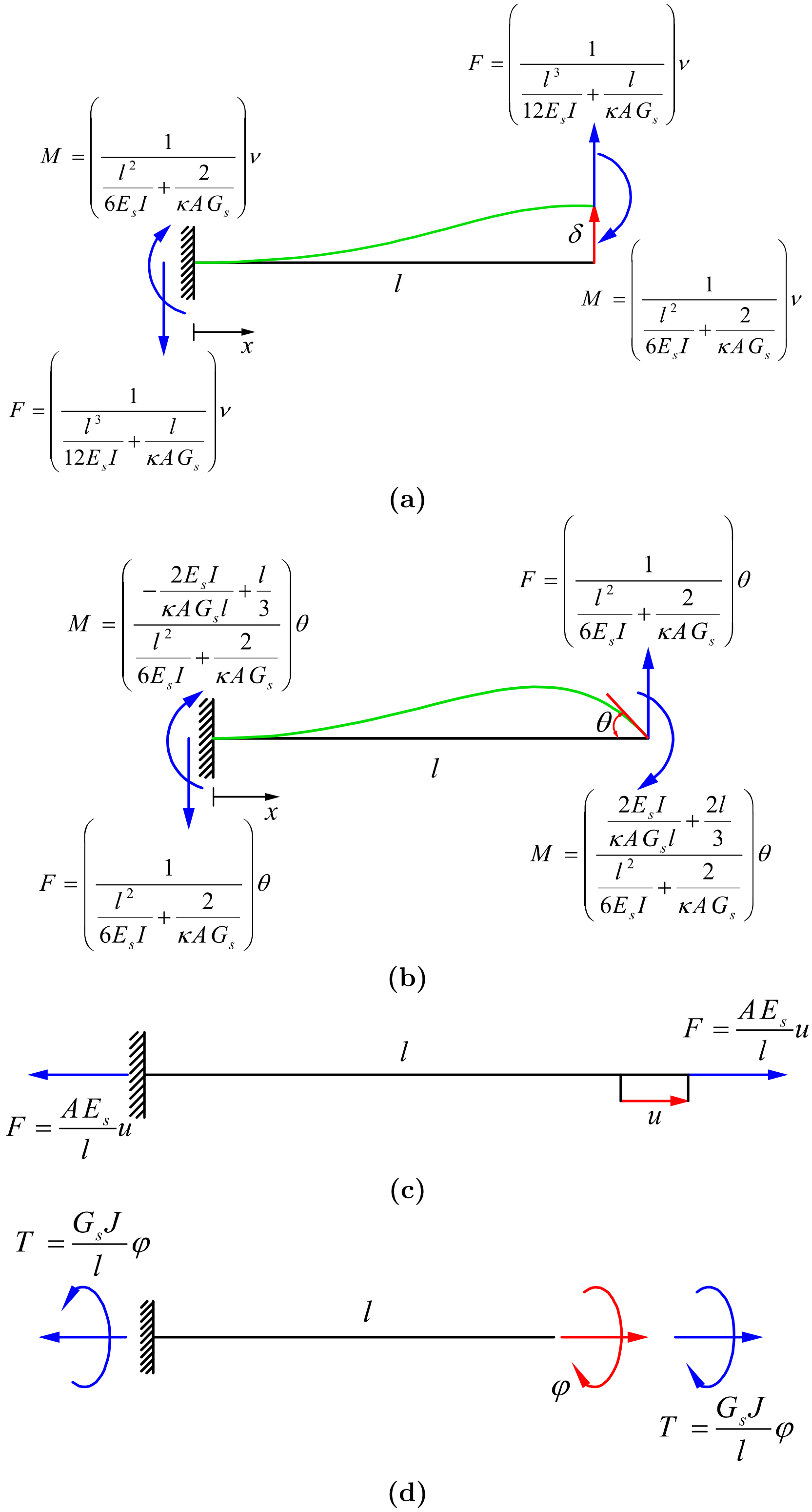

Figure 3- Forces and moments required to cause (a) lateral displacement $\boldsymbol{\delta}$ with no rotation at the free end of the beam, and (b) rotation $\boldsymbol{\theta}$ with no lateral displacement at the free end of the beam, (c) pure axial extension, and (d) pure twist in the free end of a Timoshenko beam

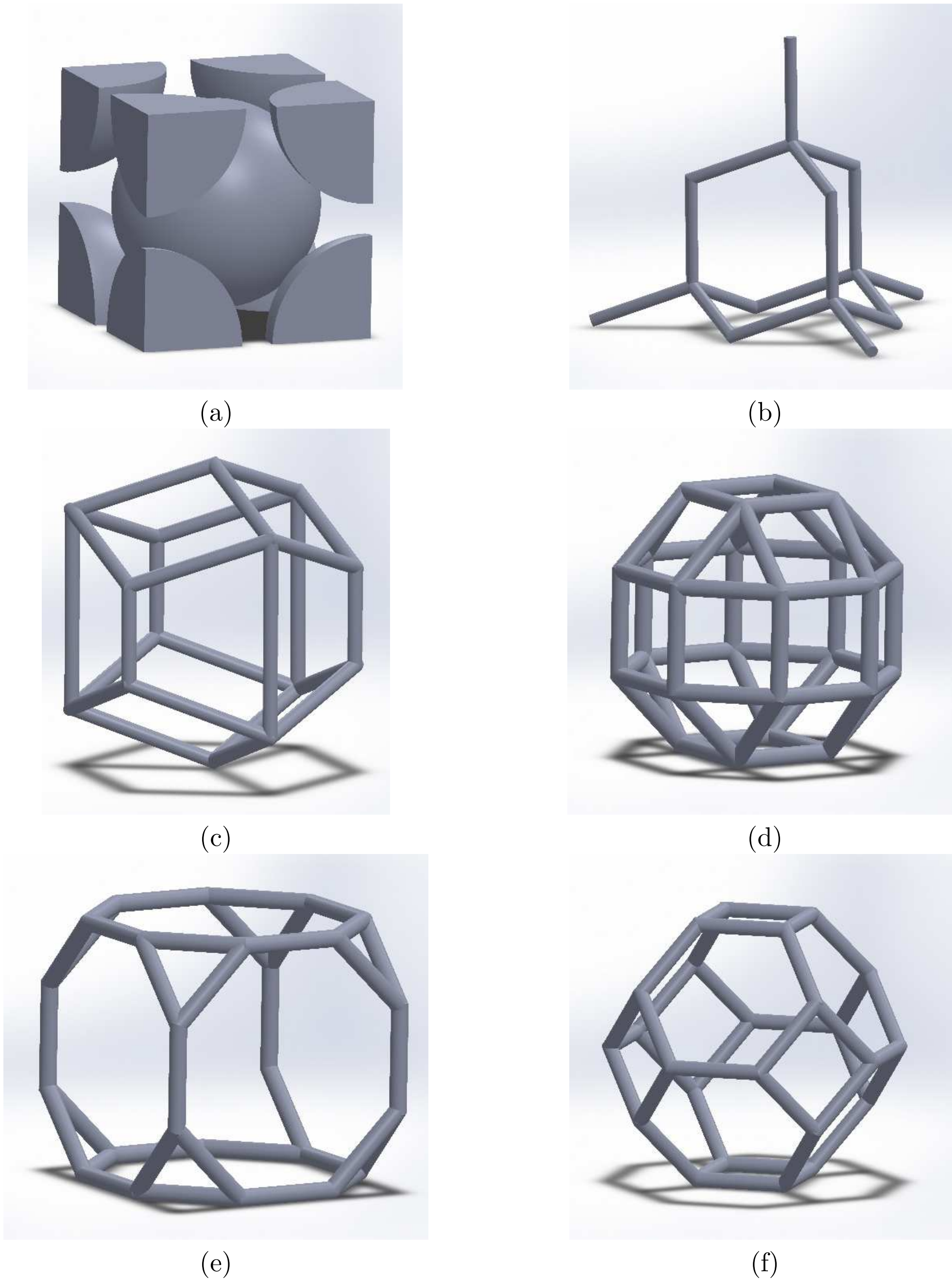

Figure 4- Unit cells of (a) BCC, (b) Diamond, (c) Hexagonal packing, (d) Rhombicuboctahedron, (e) Truncated cube, and (f) Truncated octahedron.

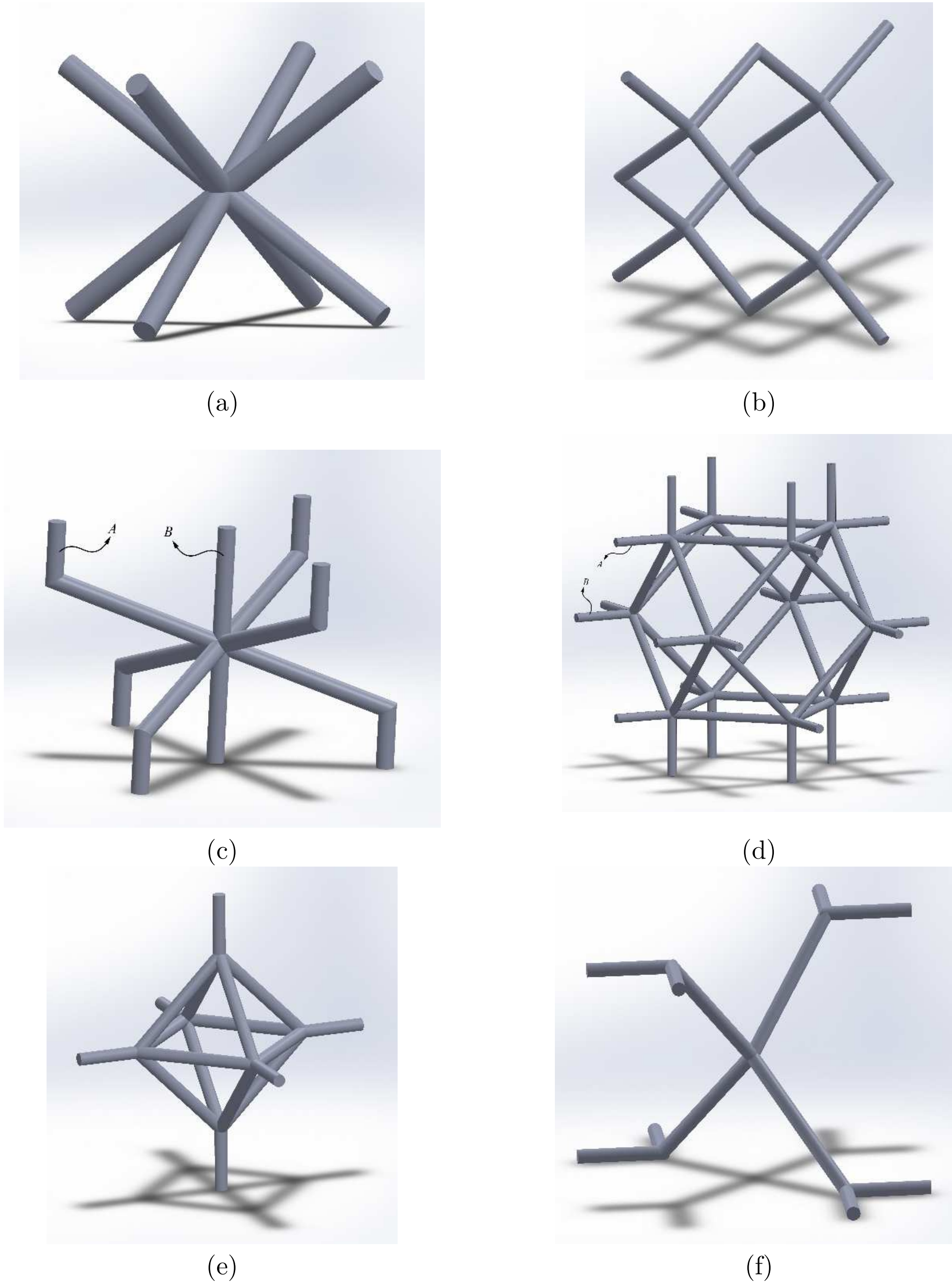

Figure 5- Unit cells used for analytical and numerical analysis: (a) BCC, (b) Diamond, (c) Hexagonal packing, (d) Rhombicuboctahedron, (e) Truncated cube, and (f) Truncated octahedron.

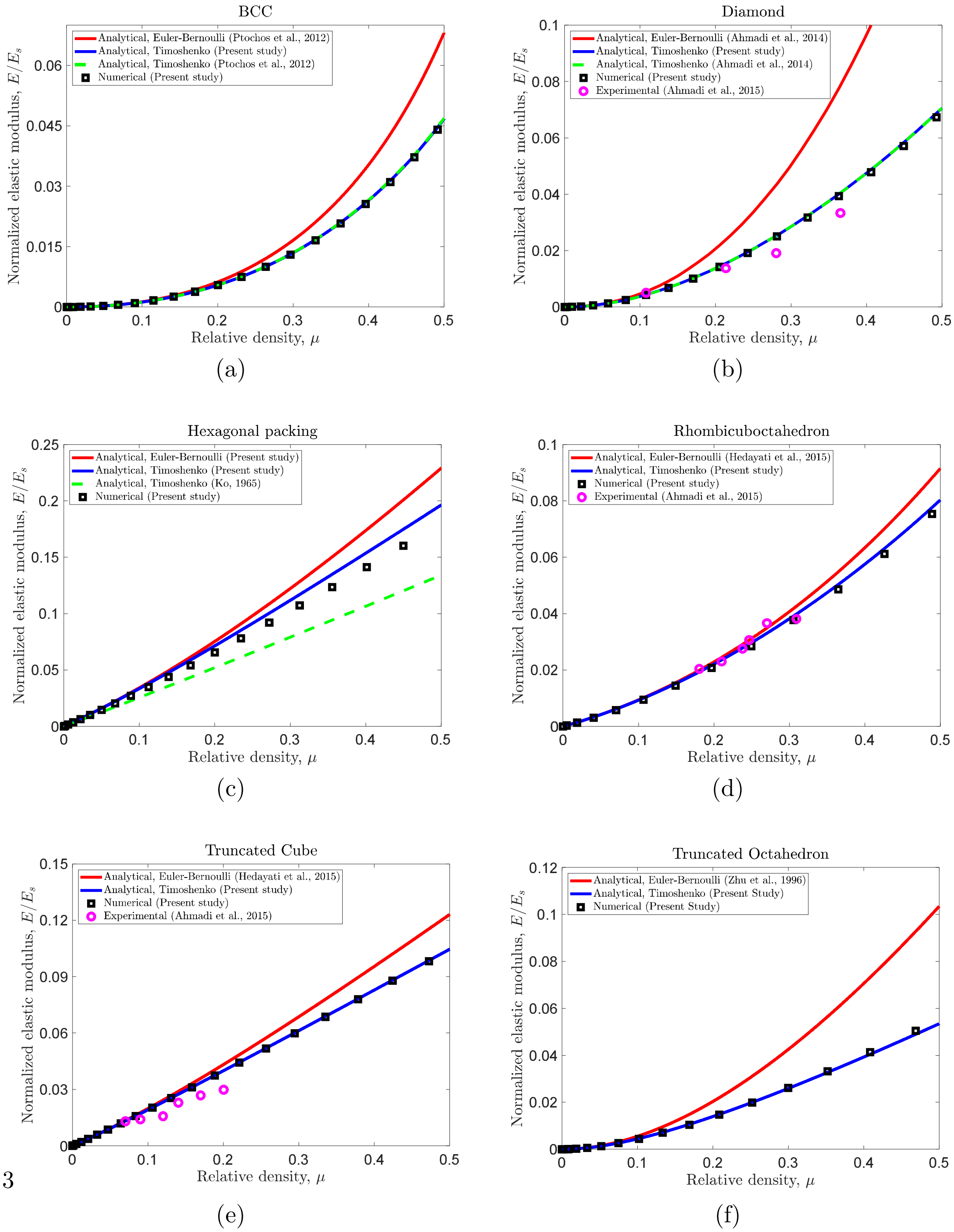

3

Figure 6- Comparison of analytical (Euler-Bernoulli and Timoshenko) and numerical values of normalized Elastic modulus for different unit cells: (a) BCC, (b) Diamond, (c) Hexagonal packing, (d) Rhombicuboctahedron, (e) Truncated cube, and (f) Truncated octahedron.

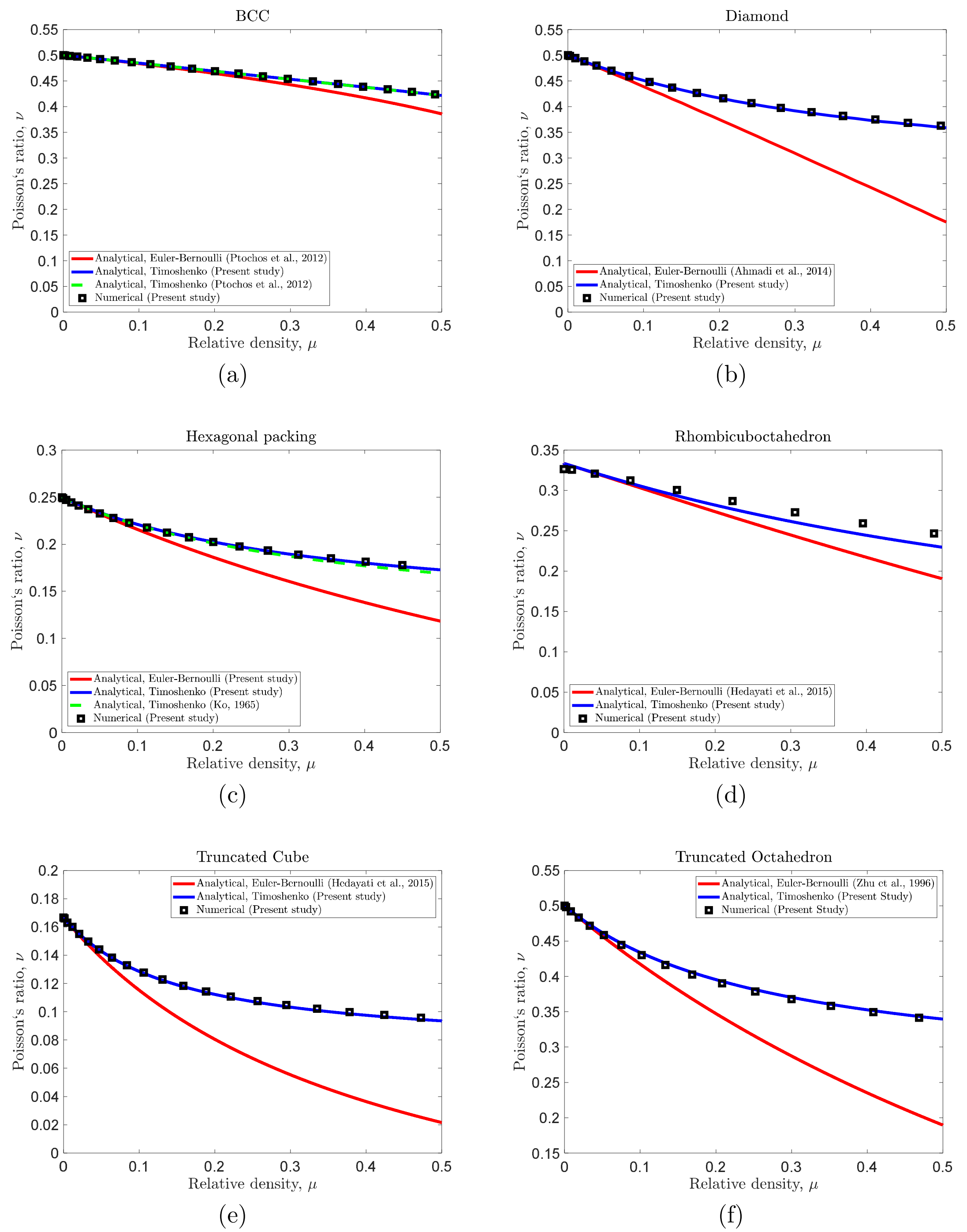

Figure 7- Comparison of analytical (Euler-Bernoulli and Timoshenko) and numerical values of Poisson's ratio for different unit cells: (a) BCC, (b) Diamond, (c) Hexagonal packing, (d) Rhombicuboctahedron, (e) Truncated cube, and (f) Truncated octahedron.

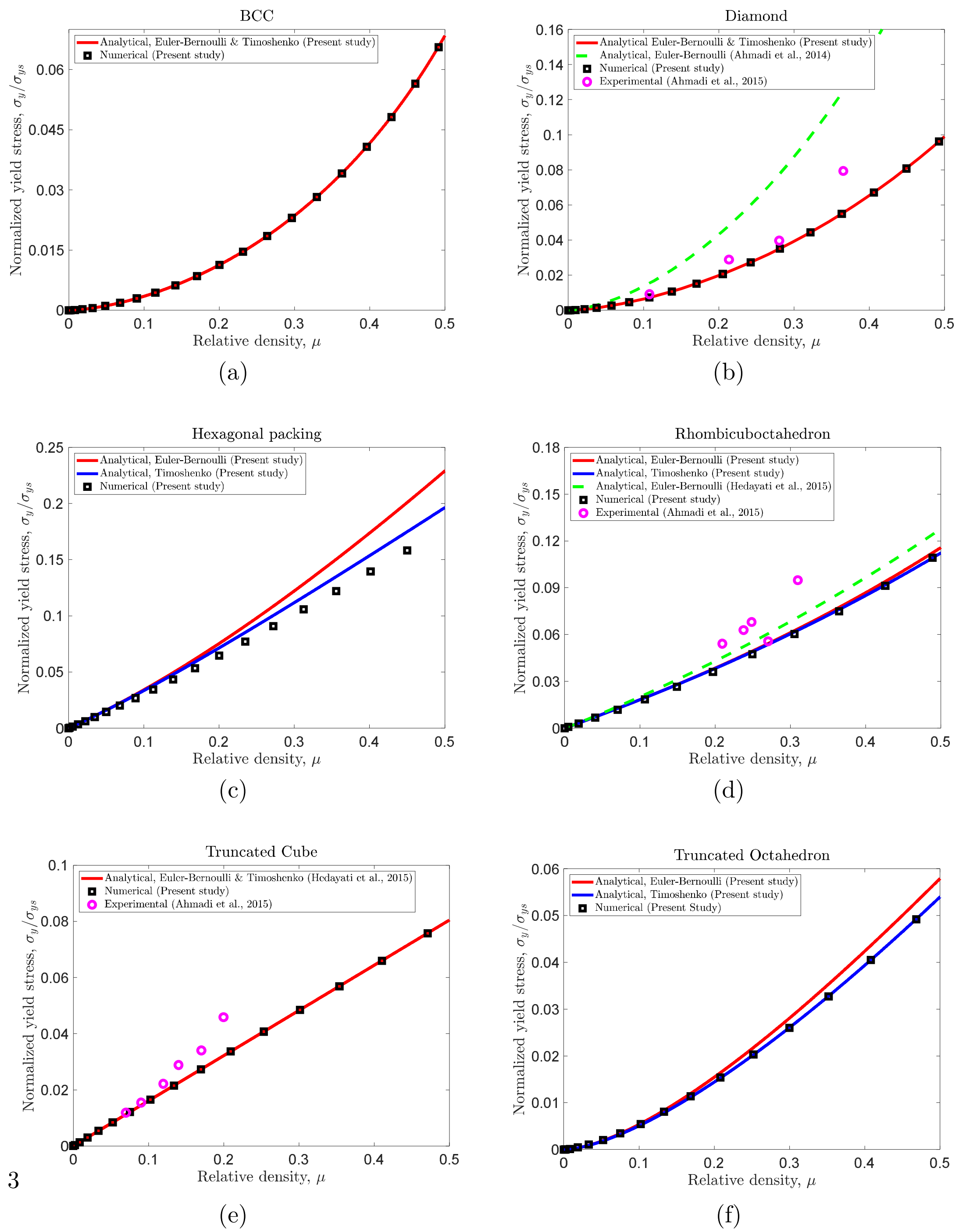

3

Figure 8- Comparison of analytical (Euler-Bernoulli and Timoshenko) and numerical values of Yield stress for different unit cells: (a) BCC, (b) Diamond, (c) Hexagonal packing, (d) Rhombicuboctahedron, (e) Truncated cube, and (f) Truncated octahedron.

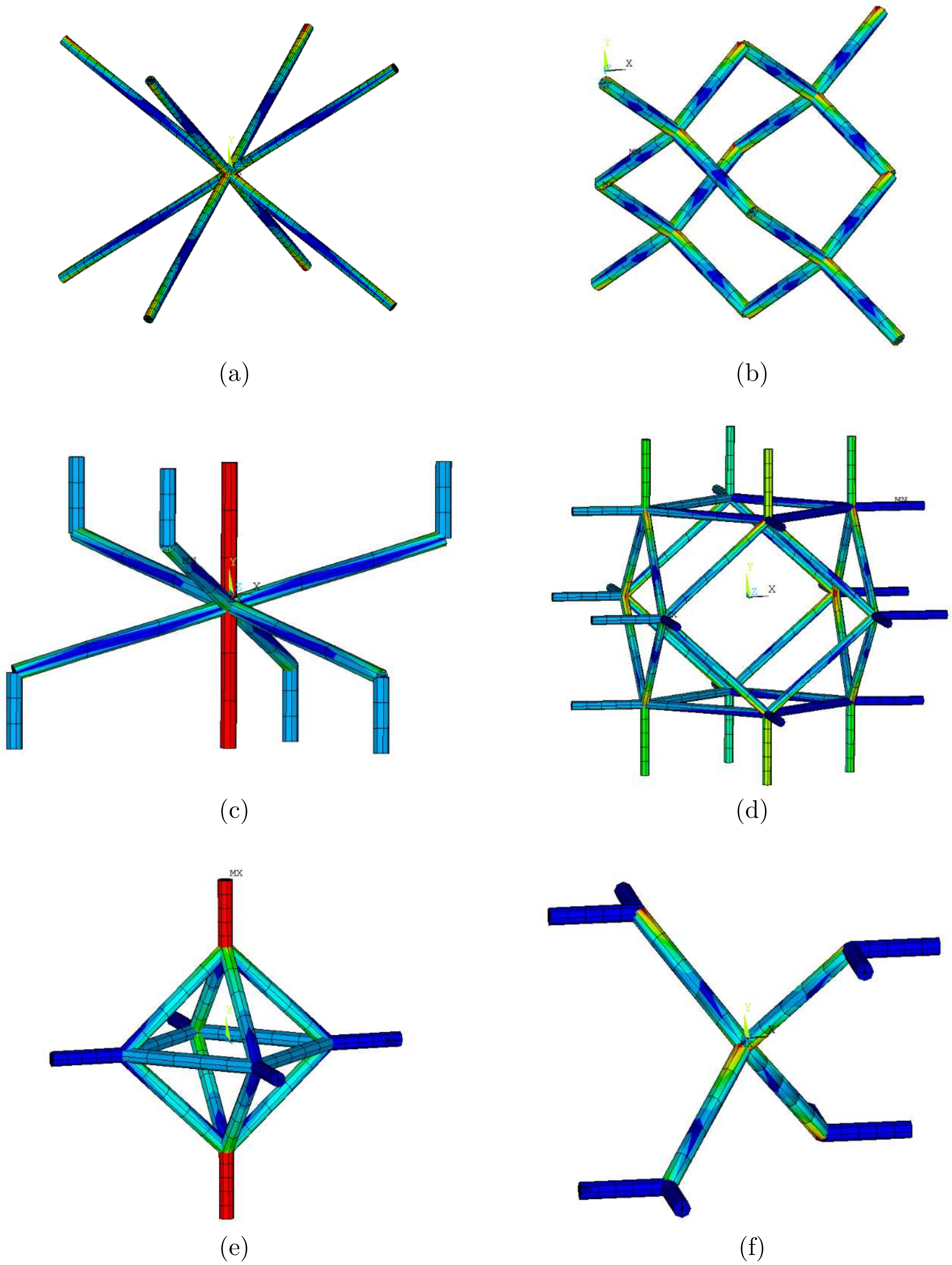

Figure 9- unit cells stress contour: (a) BCC, (b) Diamond, (c) Hexagonal packing, (d) Rhombicuboctahedron, (e) Truncated cube, and (f) Truncated octahedron.